Supporting Information

Arenz et al

SI Materials and Methods

Purification of TetM protein

Enterococcus faecalis TetM from TnFO1 (Q47810) was cloned into pET-46 Ek/LIC (Novagene) with an N-terminal 6x histidine tag. The plasmid was transformed into *E. coli* BL21(DE3) (Novagene) and incubated at 37°C/120 rpm overnight in 20 mL LB medium containing 100 μg/mL ampicillin. A volume of 20 mL overnight culture was used to inoculate 1.6 L of LB medium containing 100 μg/mL ampicillin. The culture was grown at 37°C/120 rpm to an OD_{600} of 0.3. The temperature was then reduced to 30°C and 16 mL of ethanol was added until the OD_{600} value reached 0.6. Expression of TetM was induced by adding 1.6 ml of 1mM IPTG. After 2hrs, cells were harvested by centrifugation at 3000 x g for 15 min at 4°C and subsequently resuspended in 25 mL Lysis buffer (50 mM NaH_2PO_4, 300 mM NaCl, 5 mM Imidazole, pH 8.0). Cells were lysed using the M-110L Microfluidizer (Microfluidics) and the lysate cleared by centrifugation at 17000 x g for 15 min at 4°C. The cleared lysate was then incubated at 4°C for 1h with 1 mL Ni-NTA agarose beads (Machery-Nagel) and loaded onto a 20 mL Econopac Chromatography column (Biorad). Beads were washed twice with 5 mL Wash buffer (50 mM NaH_2PO_4, 300 mM NaCl, 10 mM Imidazole, pH 8.0) and eluted in 2 mL Elution buffer (50 mM NaH_2PO_4, 300 mM NaCl, 250 mM Imidazole, pH 8.0). The eluate was further purified by gel filtration using a Superdex™ 75 pg column (Amersham) and GF buffer (50 mM Hepes, 100 mM KCl, 200 mM NaCl, 10 mM $MgCl_2$, 5 mM ß-Mercaptoethanol, 10% Glycerol).

Site directed mutagenesis

Site directed mutagenesis was performed using the whole plasmid PCR method. Primers are attached in **Supplementary Table 2**. *E. faecalis tetM* on pET-46 Ek/LIC (Novagene) was used as a template. Double mutants W442A + loop III were produced using loop III mutants as templates (1). KOD Xtreme™ Hot Start Polymerase (Novagene) was used in the following PCR program: 94°C 2 min; 20x (98°C 10sec, 63°C 30sec, 68°C 7min); 68°C 7min.

Generation and purification of ErmCL-SRC

ErmCL-SRC was generated following the same procedure as previously described (2). The *2XermCL* construct contained a T7 promoter followed by a strong ribosome binding site (RBS) spaced by 7 nucleotides (nts) to the ATG start codon of the first *ermCL* cistron. A linker of 22

nts separated the stop codon of the first *ermCL* cistron and the start codon of the second *ermCL* cistron. The linker also comprised the strong RBS 7 nts upstream of the ATG start codon of the second *ermCL* cistron, enabling initiation of translation independent from the first *ermCL* cistron. Each *ermCL* cistron encoded amino acids 1-19 corresponding to ErmCL leader peptide (Genbank accession number V01278) present on macrolide resistance plasmid pE194 (3, 4). *In vitro* translation of the *2xermCL* construct was performed using the Rapid Translation System RTS 100 *E. coli* HY Kit (Roche) and was carried-out in the presence of 10 μM erythromycin (ERY) for 1h at 30 °C. The ErmCL-SRC was purified from the disome fractions on sucrose gradients and concentrated using Amicon Ultra-0.5 mL Centrifugal Filters (Millipore). Monosomes of the ErmCL-SRC were obtained by annealing a short DNA oligonucleotide (5'-ttcctccttataaaact-3', Metabion) to the linker between the *ermCL* cistrons of the disomes, generating a DNA-RNA hybrid that was cleaved by RNase H (NEB) treatment in buffer A at 25°C for 1h. The ErmCL-SRC monosomes were then purified and concentrated using the Amicon Ultra-0.5 mL Centrifugal Filters (Millipore).

Generation of TetM●RNCs

The ErmCL-SRC (0.5 μM) was incubated with a 4-fold excess (2 μM) of purified recombinant TetM protein in the presence of 500 μM GDPCP in buffer A (50 mM HEPES-KOH, pH7.4, 100 mM KOAc, 25 mM $Mg(OAc)_2$, 6 mM β-mercaptoethanol, 100 μM evernimicin and 10 μM erythromycin) for 30 min at 30°C. Thereafter, the binding reaction was diluted using buffer A to yield a final ribosome concentration of 4 A_{260}/ml for cryo-grid preparation.

Cryo-electron microscopy and single particle reconstruction

The TetM●RNC (4 A_{260}/ml) was applied to 2 nm pre-coated Quantifoil R3/3 holey carbon supported grids and vitrified using a Vitrobot Mark IV (FEI Company). Data collection was performed using the EPU software at NeCEN (Leiden, Netherlands) on a Titan Krios transmission electron microscope (TEM) (FEI, Holland) equipped with a Falcon II direct electron detector at 300 kV with a magnification of 125,085x, a pixelsize of 1.108 Å and a defocus range of 0.9-2.2 μm. The data were provided as a series of seven frames (dose per frame is 4 $e^-/Å^2$) from which we summed frames 1-6 (accumulated dose of 24 $e^-/Å^2$) after alignment using Motion Correction software (5). Images were processed using a frequency-limited refinement protocol that helps prevent over-fitting (6), specifically by truncation of high frequencies (in this case at 7-8 Å using a Butterworth filter). Power spectra and defocus values were determined using the SPIDER TF ED command and recorded images were manually inspected for good areas and power-spectra quality. Data were processed further using the

SPIDER software package (7), in combination with an automated workflow as described previously (8). After initial, automated particle selection based on the program SIGNATURE (9), initial alignment was performed with 127,205 particles, using *E. coli* 70S ribosome as a reference structure (2). After removal of noisy particles (22,207 particles), the dataset could be sorted into two main subpopulations using an incremental K-means-like method of unsupervised 3D sorting (10): The first subpopulation (26,814 particles; 25%) was defined by the presence of stoichiometric density for P-site tRNA. The second, major subpopulation (78,186 particles; 75%) was defined by the presence of stoichiometric densities for P-tRNA and TetM (***SI Appendix*, Figure S1A**), and could be refined further to produce a map with an average resolution of 3.9 Å (0.143 FSC, ***SI Appendix*, Figure S1B**). The final refined map was subjected to the program EMBFACTOR (11) in order to apply an automatically determined negative B-factor for sharpening of the map. Local resolution calculations were performed using Resmap (12) revealing that the resolution of the majority of the core of the 30S and 50S subunits extended to 3.5 Å (***SI Appendix*, Figure S1C**).

Molecular modelling and map-docking procedures

The initial molecular model for the 70S ribosome of the TetM●RNC was based on the cryo-EM structure of an *E. coli* 70S ribosome (PDB ID 5AFI, (13)). The 30S and 50S subunits were fitted as rigid bodies and were manually adjusted and refined in Coot (14). The model for the C-terminal domain of L7 was based on a rigid body fit of the NMR structure of L7/L12 (1RQU, (15)). The molecular model for TetM was initially based on a homology model using EF-G as a template (generated by HHPred (16) and Modeller (17)). The model was split into five domains, which were individually fitted into the EM density as rigid bodies and then manually adjusted and refined using Coot (14) and PHENIX (18). Since the resolution of domains I-III and V of TetM was insufficient to model the amino acid side chains, only a backbone trace was generated. Domain IV of TetM was resolved up to 3.5 Å allowing the bulky amino acid side-chains in loop III to be modelled.

Figure preparation

Figures showing electron densities and atomic models were generated using UCSF Chimera (19) and PyMOL Molecular Graphics System (Version 1.5.0.4 Schrödinger, LLC).

Supplementary Figures

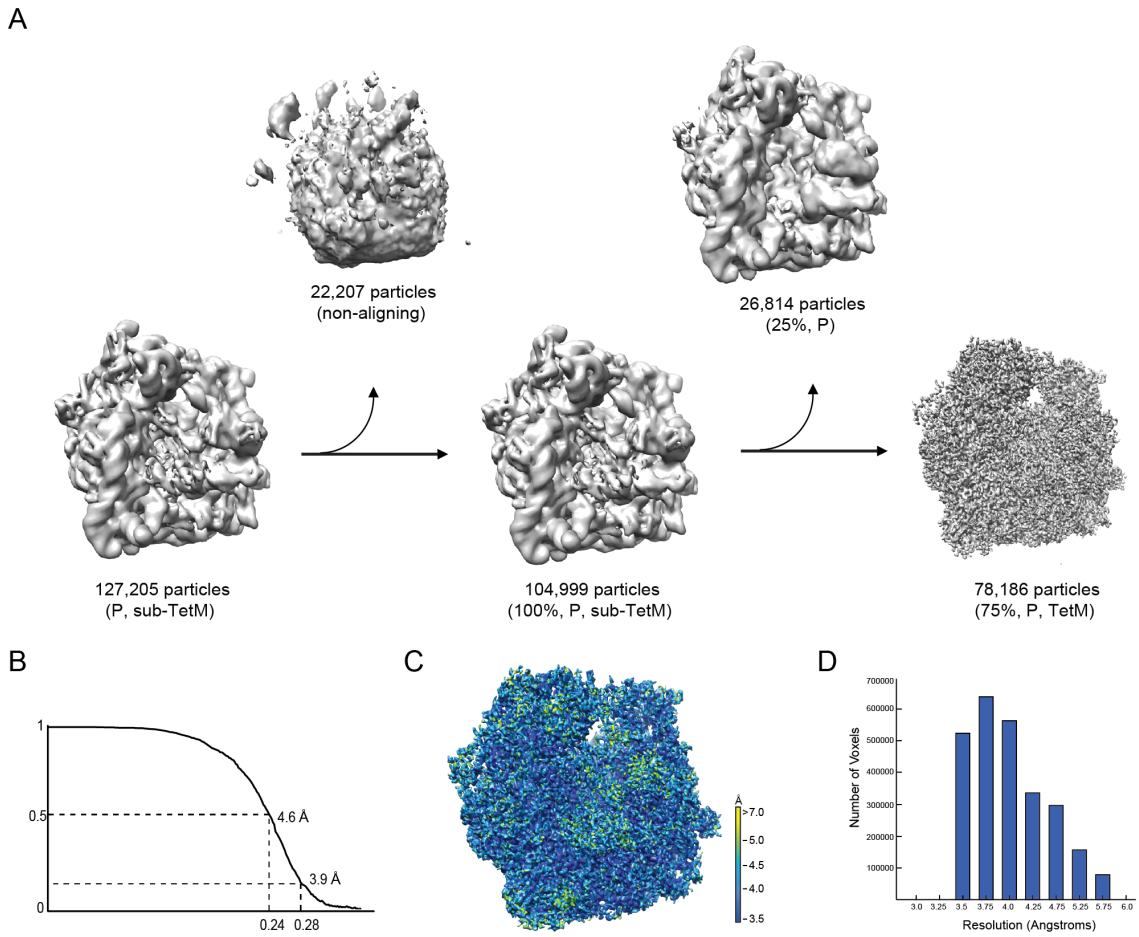

Figure S1 Cryo-EM reconstruction of the TetM•RNC. (**A**) *In silico* sorting of the TetM•RNC dataset. After removal of non-aligning and edge particles, sorting of the dataset yielded two homogenous sub-datasets. The vast majority of the particles (75%; 78,186 particles in total) contained stoichiometric density for P-tRNA as well as for TetM and this subpopulation was chosen for refinement. (**B**) Fourier-shell correlation curve of the refined final map, indicating the average resolution of the TetM•RNC is 3.9 Å. (**C**) Overview of the TetM•RNC colored according to the local resolution as calculated using ResMap (12). (**D**) Histogram generated by ResMap showing the number of voxels of the cryo-EM map of the TetM•RNC distributed across the resolution bins ranging from 3.5 Å to 6.0 Å.

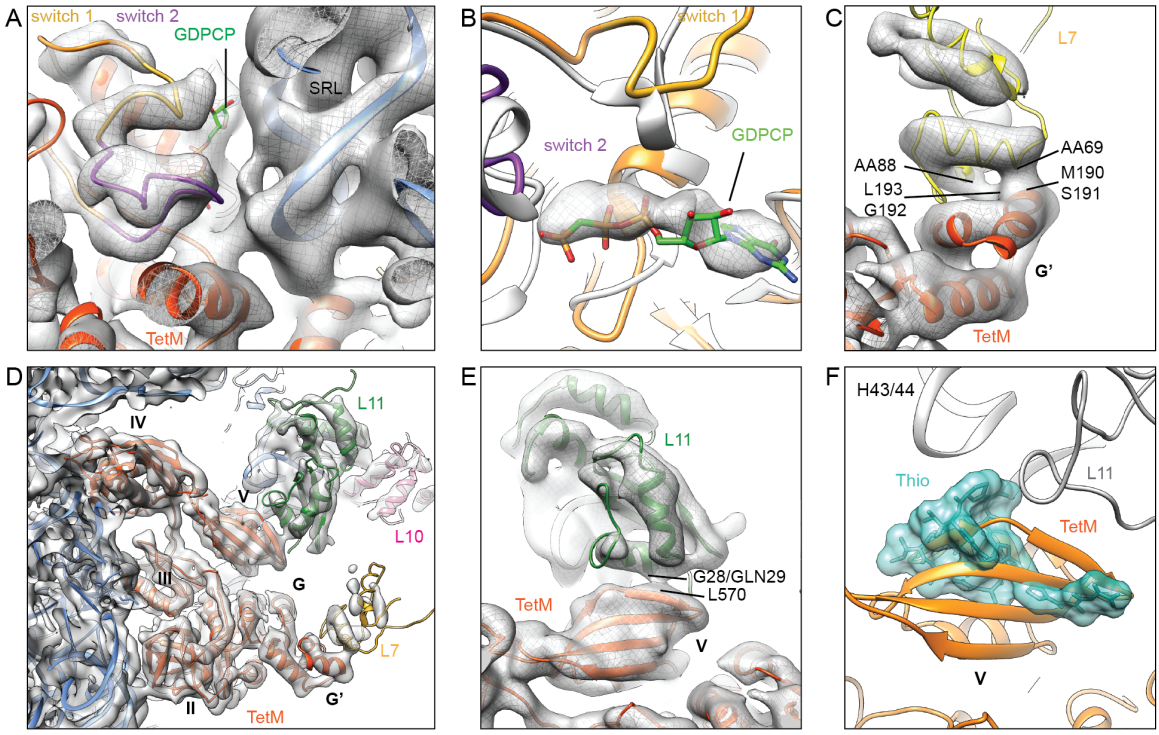

Figure S2 Interaction of TetM with the large ribosomal subunit. (**A**) Interaction of the G domain of TetM with the sarcin-ricin loop (SRL) of the 23S rRNA (blue). The switch 1 (yellow) and switch 2 (purple) loops are indicated, as is the putative position for the GDPCP molecule (green). (**B**) Comparison of the conformation of switch 1 and 2 loops of TetM with equivalent region of EF-G (PDB ID 4CR1). Putative density for GDPCP molecule (grey mesh) corresponds with the position of the GDPNP molecule (green) from the EF-G structure (PDB ID 4CR1) aligned to the TetM based on the G domain. (**C**) Interaction between the C-terminal domain of L7/L12 (yellow) and the G' domain of TetM (orange). (**D**) Overview of TetM (orange) showing interaction with L7 (yellow) and L11 (green). (**E**) Interaction between L11 (green) and domain V of TetM (orange). (**F**) Overlap in the binding site of domain V of TetM (orange) with the antibiotic thiostrepton (cyan). In panels (A) and (C-E), the cryo-EM density for the TetM-RNC is shown as a grey mesh.

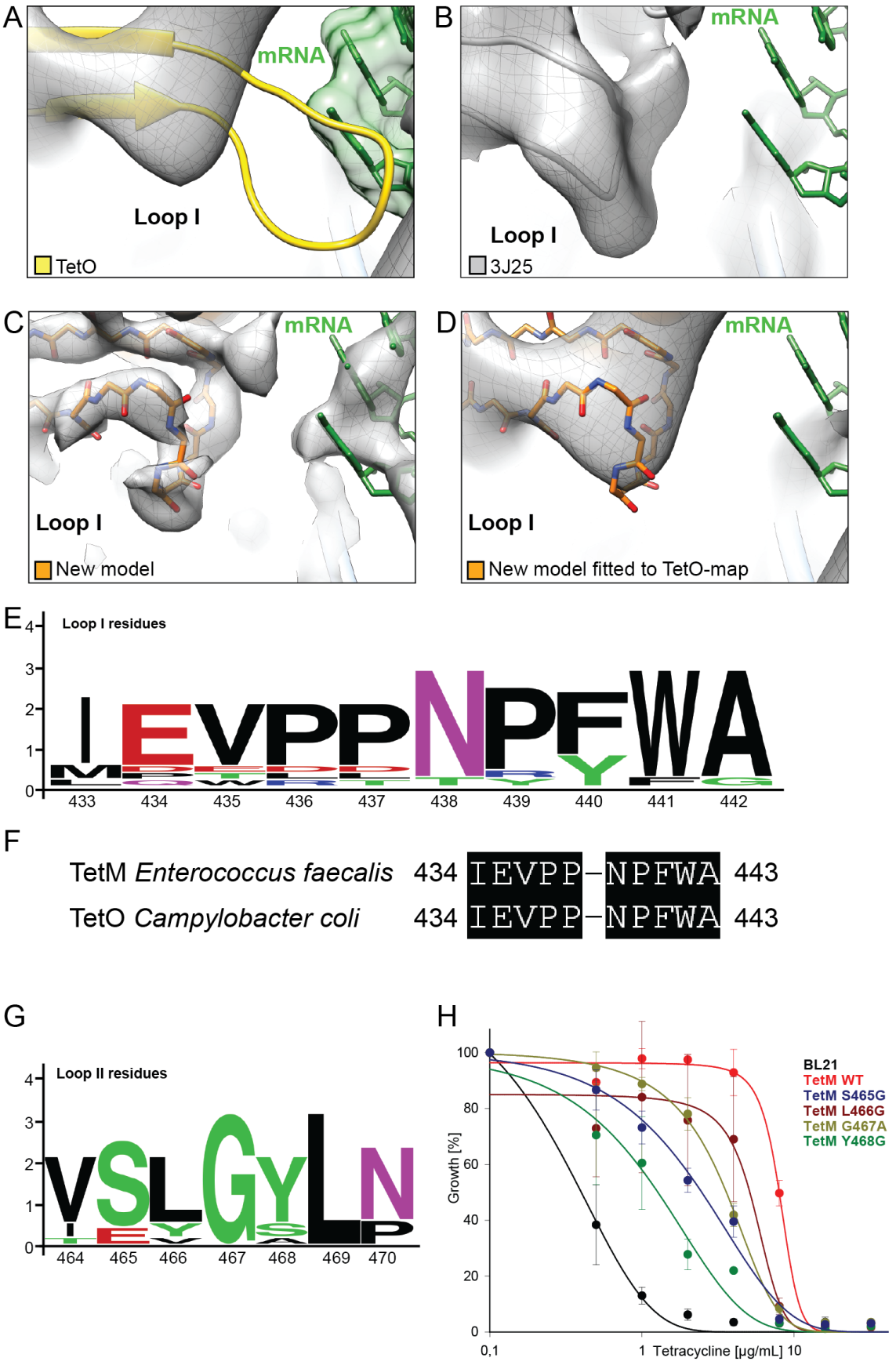

Figure S3 Analysis of loops I and II of domain IV of TetM. (**A-D**) Cryo-EM map (grey mesh) of (**A, D**) TetO•70S complex (20), (**B**) TetM•70S complex (1) and (**C**) TetM•RNC, with molecular model for loop I of domain IV of (**A**) TetO (yellow, (20)), (**B**) TetM (grey, PDB

3J25, (1)) and (**C, D**) the revised molecular model for loop I of domain IV of TetM based on the cryo-EM map of the TetM•RNC at 3.9 Å resolution (orange). (**E**) Logo-Plot of residues 433-443 of loop I of domain IV of TetM, numbered according to *Enterococcus faecalis* TetM. (**F**) Sequence alignment of residues 433-443 of loop I of *Enterococcus faecalis* TetM and *Campylobacter coli* TetO. (**G**) Logo-plot of residues 464-470 forming loop II of TetM domain IV. (**H**) Growth curves of wildtype *E. coli* strain BL21 (black) in the presence of increasing concentrations of tetracycline (0-128 μg/ml) compared with the wildtype strain harboring a plasmid encoding wildtype TetM (red) or TetM single mutants S465G (blue), L466G (brown), G467A (olive) and Y468G (green).

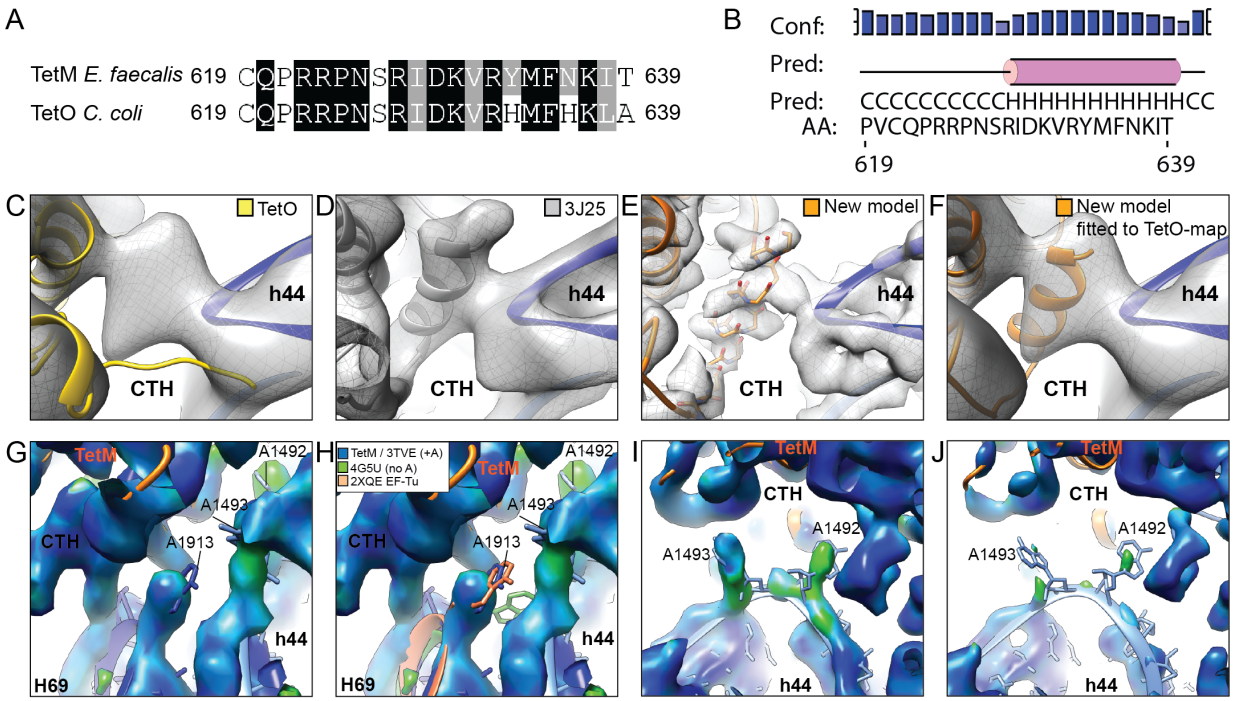

Figure S4 Interaction of the C-terminal helix of TetM with the ribosomal decoding center

(**A**) Sequence alignment of residues 619-639 of the C-terminal helix (CTH) of *Enterococcus faecalis* TetM and *Campylobacter coli* TetO. (**B**) PSIPRED secondary structure prediction with sequence (AA), prediction (Pred) and confidence (Conf) as indicated. (**C-F**) Cryo-EM map (grey mesh) of (**C, F**) TetO•70S complex (20), (**D**) TetM•70S complex (1) and (**E**) TetM•RNC, with molecular model for the CTH of (**C**) TetO (yellow, (20)), (**D**) TetM (grey, PDB 3J25, (1)) and (**E, F**) the revised molecular model for loop I of domain IV of TetM based on the cryo-EM map of the TetM•RNC at 3.9 Å resolution (orange). (**G-I**) Identical views as **Fig. 2C-F** but including electron density colored according to the local resolution. (**J**) As (I) but with a higher threshold level for the electron density map.

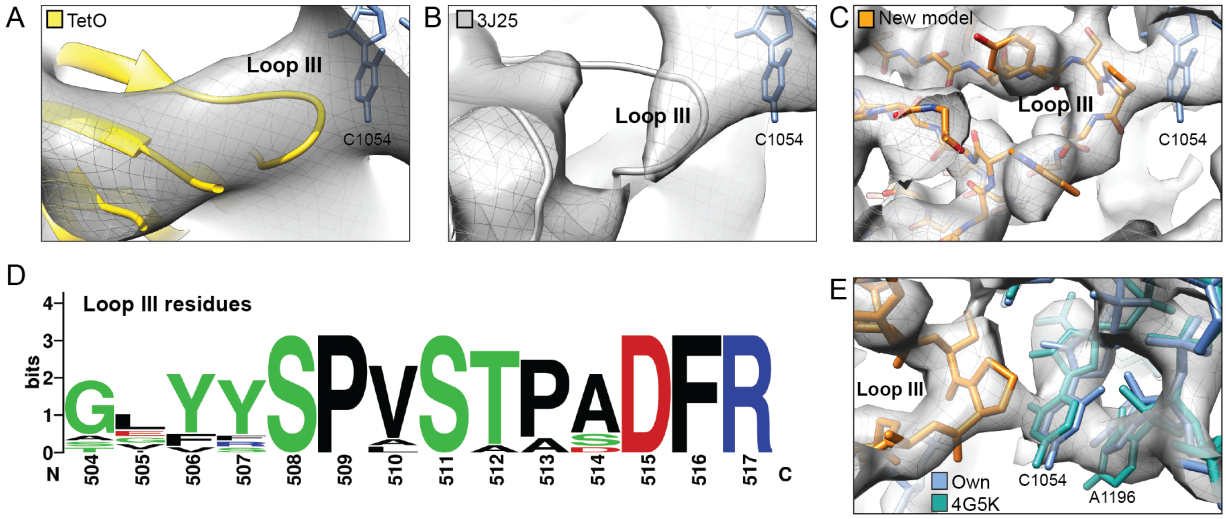

Figure S5 Structures of loop III of domain IV in TetO and TetM. (**A-C**) Cryo-EM map (grey mesh) of (**A**) TetO•70S complex (20), (**B**) TetM•70S complex (1) and (**C**) TetM•RNC, with molecular model for loop III of domain IV of (**A**) TetO (yellow, (20)), (**B**) TetM (grey, PDB 3J25, (1)) and (**C**) the revised molecular model for loop I of domain IV of TetM based on the cryo-EM map of the TetM•RNC at 3.9 Å resolution (orange). (**D**) Logo-Plot of residues 504-517 of loop III of domain IV of TetM, numbered according to *Enterococcus faecalis* TetM. (**E**) Cryo-EM density (grey mesh) the TetM•RNC with molecular models for TetM (orange), and a comparison of the conformation of C1054 of the 16S rRNA from the TetM•RNC (blue) with the tetracycline-bound conformation (cyan, (21)).

Supplementary Table 1

TetM			Ribosome	
Domain	**Region**	**Residue**	**Region**	**Residue**
G				
	loop between 1_1 and A_1	V12	23S rRNA, H95 (SRL)	G2661
	loop between A_1 and 2_1	G53	23S rRNA, H95 (SRL)	G2663
	loop between 3_1 and B_1	H78	23S rRNA, H95 (SRL)	A2662
	loop between 4_1 and C_1	K102	23S rRNA, H95 (SRL)	A2657
	C1	A107	23S rRNA, H95 (SRL)	G2661
	loop between 5_1 and D_1	Q132	23S rRNA, H95 (SRL)	A2657
	loop between 5_1 and D_1	G134	L6	V91, G92
G'	B_G	M190,S191	L7-CTD, helix α4	V69
	B_G	G192,L193	L7-CTD, helix α4	V88
II	3_2	R278	16S rRNA, h5 (body)	U368
	5_2	T292	16S rRNA, h5 (body)	U358
	6_2	L304	16S rRNA, h5 (body)	A55
III	A_3	D363	S12	H77
IV	**loop II** between 4_4 and A_4	S465, L466, G467	16S rRNA, h34 (head)	backbone C1214, C1209, C1051
	loop III between 5_4 and B_4	Y506, S508, P509	16S rRNA, h34 (head)	backbone C1051 U1052, C1054
	loop III between 5_4 and B_4	P513	16S rRNA, h18 (body)	C518
	loop III between 5_4 and B_4	R517	16S rRNA, h18 (body)	C519
V	A5	Y555	23S rRNA, H43/H44	A1095
	A5	K560	23S rRNA, H89	U2473
	2_5	L570	L11 3_{10}-helix	G28, Q29
	B5	T594, F595	L6	K175, K176
	B5	T594, F595	23S rRNA, H95 (SRL)	A2660
	B5	N598, G599	23S rRNA, H95 (SRL)	A2660
CTE	loop between 4_5 and C_5	R627	S12	L49
	C_5	R632	23S rRNA, H69	C1913
	C_5	F635, N636	23S rRNA, H69	C1914

Supplementary Table 2

Construct	Primer sense/ antisense (5’ – 3’)
TetM W442A	5’-GTGCCGCCAAATCCTTTCGCGGCTTCCATTGGTTTATCTGTATCACCGCTTC-3’ 5’-GATAAACCAATGGAAGCCGCGAAAGGATTTGGCGGCACTTCGATGTGAATG-3’
TetM S465G	5’-CAGTATGAGAGCTCGGTTGGCCTTGGATACTTAAATCAATCATTTC-3’ 5’-GATTTAAGTATCCAAGGCCAACCGAGCTCTCATACTGCATTCCAC-3’
TetM L466G	5’-GAGAGCTCGGTTTCTGGCGGATACTTAAATCAATCATTTCAAAATG-3’ 5’-GATTGATTTAAGTATCCGCCAGAAACCGAGCTCTCATACTGCATTC-3’
TetM G467A	5’-GAGCTCGGTTTCTCTTGCGTACTTAAATCAATCATTTCAAAATGCAG-3’ 5’-GAAATGATTGATTTAAGTACGCAAGAGAAACCGAGCTCTCATACTGCATTC-3’
TetM Y468G	5’-CTCGGTTTCTCTTGGAGGCTTAAATCAATCATTTCAAAATGCAG-3’ 5’-GAAATGATTGATTTAAGCCTCCAAGAGAAACCGAGCTCTCATAC-3’
TetM F516A	5’-GTTAGTACCCCAGCAGATGCGCGGATGCTTGCTCCTATTGTATTGGAAC-3’ 5’-CAATAGGAGCAAGCATCCGCGCATCTGCTGGGGTACTAACAGGGCTATAG-3’
TetM F516D	5’-GTTAGTACCCCAGCAGATGATCGGATGCTTGCTCCTATTGTATTGGAAC-3’ 5’-CAATAGGAGCAAGCATCCGATCATCTGCTGGGGTACTAACAGGGCTATAG-3’

References

1. Dönhöfer A, *et al*. (2012) Structural basis for TetM-mediated tetracycline resistance. *Proc. Natl. Acad. Sci. USA* 109(42):16900-16905.
2. Arenz S, *et al*. (2014) Drug Sensing by the Ribosome Induces Translational Arrest via Active Site Perturbation. *Mol Cell* 56(3):446-452.
3. Iordanescu S (1976) Three distinct plasmids originating in the same Staphylococcus aureus strain. *Archives roumaines de pathologie experimentales et de microbiologie* 35(1-2):111-118.
4. Narayanan CS & Dubnau D (1985) Evidence for the translational attenuation model: ribosome-binding studies and structural analysis with an in vitro run-off transcript of ermC. *Nucleic Acids Res* 13(20):7307-7326.
5. Li X, *et al*. (2013) Electron counting and beam-induced motion correction enable near-atomic-resolution single-particle cryo-EM. *Nat Methods* 10(6):584-590.
6. Scheres SH & Chen S (2012) Prevention of overfitting in cryo-EM structure determination. *Nat Methods* 9(9):853-854.
7. Frank J, *et al*. (1996) SPIDER and WEB: processing and visualization of images in 3D electron microscopy and related fields. *J Struct Biol* 116(1):190-199.
8. Becker T, *et al*. (2012) Structural basis of highly conserved ribosome recycling in eukaryotes and archaea. *Nature* 482(7386):501-506.
9. Chen JZ & Grigorieff N (2007) SIGNATURE: a single-particle selection system for molecular electron microscopy. *J. Struct. Biol.* 157(1):168-173.
10. Loerke J, Giesebrecht J, & Spahn CM (2010) Multiparticle cryo-EM of ribosomes. *Methods Enzymol* 483:161-177.
11. Fernandez JJ, Luque D, Caston JR, & Carrascosa JL (2008) Sharpening high resolution information in single particle electron cryomicroscopy. *J Struct Biol* 164(1):170-175.
12. Kucukelbir A, Sigworth FJ, & Tagare HD (2014) Quantifying the local resolution of cryo-EM density maps. *Nat Methods* 11(1):63-65.
13. Fischer N, *et al*. (2015) Structure of the E. coli ribosome-EF-Tu complex at <3 A resolution by C-corrected cryo-EM. *Nature*.
14. Emsley P & Cowtan K (2004) Coot: Model-Building Tools for Molecular Graphics. *Acta Crystallographica Section D - Biological Crystallography* 60:2126-2132.
15. Bocharov EV, *et al*. (2004) From structure and dynamics of protein L7/L12 to molecular switching in ribosome. *J. Biol. Chem.* 279(17):17697-17706.
16. Soding J, Biegert A, & Lupas AN (2005) The HHpred interactive server for protein homology detection and structure prediction. *Nucleic Acids Res* 33(Web Server issue):W244-248.
17. Eswar N, Eramian D, Webb B, Shen MY, & Sali A (2008) Protein structure modeling with MODELLER. *Methods Mol Biol* 426:145-159.
18. Adams PD, *et al*. (2010) PHENIX: a comprehensive Python-based system for macromolecular structure solution. *Acta Crystallogr D Biol Crystallogr* 66(Pt 2):213-221.
19. Pettersen EF, *et al*. (2004) UCSF Chimera - A Visualization System for Exploratory Research and Analysis. *J. Comput. Chem.* 25(13):1605-1612.
20. Li W, *et al*. (2013) Mechanism of tetracycline resistance by ribosomal protection protein Tet(O). *Nat. Commun.* 4:1477.
21. Jenner L, *et al*. (2013) Structural basis for potent inhibitory activity of the antibiotic tigecycline during protein synthesis. *Proc Natl Acad Sci U S A* 110(10):3812-3816.